Soft Matter

PAPER

View Article Online
View Journal

Cite this: DOI: 10.1039/d5sm00180c

The size ratio effect on the microstructure and magnetization of a bidisperse magnetic colloidal suspension†

Luis R. Pérez-Marcos, [a] Ronal A. DeLaCruz-Araujo, [bc] Heberth Diestra-Cruz, [d] Obidio Rubio, [e] Ubaldo M. Córdova-Figueroa [f] and Glenn C. Vidal-Urquiza *[g]

This research examines how the size ratio influences the microstructure and time-dependent magnetization in a bidisperse magnetic colloidal suspension under a uniform magnetic field. Two types of particles model the bidisperse suspension: the small particles of radius R_s and the large particles of radius R_l. The size ratio, $\xi = R_l/R_s$, defines the particle size difference. The total volume fraction of the suspension, ϕ, is obtained from $\phi = \phi_s + \phi_l$, where ϕ_s and ϕ_l are the volume fractions of the small and large particles, respectively. The magnetic dipole–dipole interaction among the small particles and the large ones is characterized by the dipolar coupling parameters λ_s and λ_l, respectively. The interactions among the applied magnetic field and the magnetic dipoles of the small and large particles are measured by the Langevin parameters α_s and α_l, respectively. This study performs Brownian dynamics (BD) simulations of a bidisperse suspension comprising $N = 1000$ particles, with $\phi = 10^{-3}$ and $\phi_s = \phi_l = 5 \times 10^{-4}$. Also, α_s ranges from 0 to 1000, and λ_s from 5 to 30. The size ratio, ξ, takes values of 1, 2 and 3. The values of λ_l and α_l are computed by the parameters aforementioned by assuming that all particles exhibit the same saturation magnetization. Our results show a rich variability in the microstructure as ξ increases. As the large particles increase in size, they exhibit a greater magnetic dipole moment, which induces a non-uniform local magnetic field around them. The surrounding small particles then aggregate with the large ones, driven by this local magnetic field. Small α_s values lead to the formation of flux-closure structures such as rings of small and large particles as well as shell-like structures, which consist of small particles surrounding the large ones. The formation of these microstructures directly affects time-dependent magnetization of the suspension, which exhibits a decay with time in the limit of long times. These findings have important implications for synthesizing magnetic colloidal suspensions with enhanced properties.

Received 19th February 2025,
Accepted 20th June 2025

DOI: 10.1039/d5sm00180c

rsc.li/soft-matter-journal

1 Introduction

A magnetic colloidal suspension is a dispersion of very small magnetic particles immersed in a non-magnetic carrier fluid.[1] Generally, these particles are covered by thixotropic agents or surfactant molecules[2–5] in order to avoid particle aggregation caused by attractive short-range interactions as a consequence of their tiny sizes. Also, because of these small sizes, the particles exhibit Brownian motion originating from random collisions between them and the molecules of the carrier fluid.[6–8]

The magnetic nature of the particles relies on the formation of magnetic multi-domains within them. However, when the particle size ranges from 20 nm to 100 nm approximately, these multi-domains are reduced to mono- or single-domains that lock onto the particle (single-domain ferromagnetic behavior).[9,10] Hence, each particle bears an intrinsic magnetic dipole moment rigidly fixed at its center of mass, which constitutes the target system of this work.

Particles interact with each other because of their dipole magnetic moments. Depending on the interaction strength,

[a] Graduate School, Master Program in Mathematical Engineering, National University of Trujillo, Trujillo, La Libertad, Peru
[b] Department of Civil Engineering, National Autonomous University of Tayacaja Daniel Hernández Morillo, Tayacaja, Huancavelica, Peru
[c] SUBE program, Cesar Vallejo University, Trujillo, La Libertad, Peru
[d] Alexander Graham Bell Private Educational Institution, Trujillo, La Libertad, Peru
[e] Department of Physics and Mathematics Sciences, National University of Trujillo, Trujillo, La Libertad, Peru
[f] Department of Chemical Engineering, University of Puerto Rico–Mayagüez, Mayagüez, PR 00681, USA
[g] Department of Mechanical Engineering, Polytechnic University of Puerto Rico, San Juan, PR 00918, USA. E-mail: gvidal@pupr.edu

† Electronic supplementary information (ESI) available. See DOI: https://doi.org/10.1039/d5sm00180c

this can lead to a self-assembled aggregation (or clustering) process into structures commonly called clusters.[11–14] For instance, for dipole moments located at the center of mass, particles typically assemble into clusters arranged in a head-to-tail configuration, resulting in chain-like or ring-like structures.[15–20]

The clustering process and the morphology of the resulting clusters can also be influenced by other factors, such as the particle volume fraction in the suspension,[21,22] the application of an external magnetic field,[23–25] the application of a shear flow,[26–28] *etc.* The resulting variability in the microstructural behavior in the suspensions leads to modification of its macroscopic properties including optical (birefringence),[29–31] rheological (viscosity, yield stress, *etc.*)[32–37] and magnetic (magnetization and magnetic susceptibility) properties.[17,38–40] Therefore, by steering the microstructure suspension, the magnetic colloidal suspensions can become tunable, which allows them to be used as the working fluid in several devices for engineering (*e.g.* shock absorbers[41–43] and anti-seismic devices[44–46]) and biomedical (*e.g.* drug-delivery systems[47] and tumor removal[48]) applications.

As a result, numerous studies have been carried out using experimental and theoretical approaches. Many of them have demonstrated variability in the behavior of these suspensions that can be achieved by controlling the characteristics and functionalities of the constituent particles.[49–51] One such characteristic is the polydispersity of particle size, commonly present in realistic systems.[52] It is known that polydispersity exerts an influence on the morphology of the microstructure.[53–55] Likewise, there are improved macroscopic responses in polydisperse suspensions[56–61] relative to those without polydispersity (monodisperse suspensions).

Due to the complexity introduced by polydispersity, it is common to model it in theoretical studies through simplified approaches, such as bidispersity.[62–65] This considers the suspension to be composed of a population of small and large particles. Then, studies using this model have revealed the role of both small and large particles in microstructure formation[66–70] and the effect of bidispersity on magnetic properties, such as magnetization.[71,72] However, despite these findings, the explored systems involved particles with weak magnetic interactions, with limited attention given to the temporal evolution of both the microstructure and magnetic behavior. Thus, this has become the focus of this work, as the authors believe that it may guide the synthesis of magnetic colloidal suspensions with enhanced properties.

In this study, a simplified generalized model of a bidisperse magnetic colloidal suspension is employed to investigate the influence of bidispersity on the microstructure and magnetization of such suspensions. The study was conducted in the dilute regime under strong magnetic dipolar interparticle interactions and in the presence of a uniform magnetic field. This bidisperse model takes into account small magnetic particles of size R_s and large magnetic particles of size R_l. The size ratio $\xi = R_l/R_s$ is introduced to quantify the bidispersity of the particle size. This work is then mainly focused on two aspects. First, the effect of ξ on the development of the microstructure in bidisperse systems is observed. This microstructure is qualitatively analyzed through direct observation from simulations for different magnetic dipole–dipole interactions and magnetic field strengths. In addition, a simple quantitative analysis is carried out through the calculation of the radial distribution function of the small particles around the large ones at different stages of the clustering process. Second, the influence of the microstructure (developed in the bidisperse suspensions) on the time-dependent magnetization of these systems is investigated. To perform analysis of these aspects, the Brownian dynamics (BD) simulation method is developed to track the dynamics of the translational and rotational motion of the particles comprising the bidisperse suspension model. However, to independently assess the influence of the size ratio on the clustering process and magnetization, simulations have been conducted in the dilute regime.

The sections in this work are organized as follows: the description of the bidisperse suspension model is presented in Section 2. In Section 3, the BD simulation method is developed, where the evolution equations are derived for the linear (translation) and angular (rotation) of the small and large particles. In Section 4, the radial distribution function is defined, whereas magnetization is shown in terms of dimensionless quantities, such as the size ratio (ξ), the particle volume fractions, the dipolar coupling parameters and the Langevin parameters. In Section 5, results of the microstructure and time-dependent magnetization of the suspension are presented for different values of the simulation parameters. Finally, the conclusions are presented in Section 6.

2 Bidisperse suspension model

The model comprises two distinct categories of rigid spherical magnetic colloidal particles—small and large—suspended within a quiescent, incompressible Newtonian fluid subject to a constant magnetic field $\mathbf{H}$. These particles differ in size according to their corresponding radii R_s and R_l, as illustrated in Fig. 1. In addition, they exhibit single-domain ferromagnetic behavior, modeled as a permanent magnetic dipole moment fixed at their center, denoted by $\mathbf{m}_s$ and $\mathbf{m}_l$, respectively. These dipole moments permit interaction between the particles and each particle with the magnetic field. Here, it is considered that the magnetic dipoles are aligned along the x'-axis of a rigid-body reference frame x'–y'–z'. The magnetic field $\mathbf{H}$ is applied along the z-axis of a laboratory reference frame x–y–z, as illustrated in Fig. 1.

3 Brownian dynamics simulations

The Brownian dynamics (BD) simulation method takes into account the force and torque balance acting on colloidal particles by means of the Langevin equations approach.[73] The terms related to particle inertia are negligible because the numerical resolution timescale to solve the equations is significantly larger than the translational and rotational particle inertial relaxation times. Then, assuming that the suspension

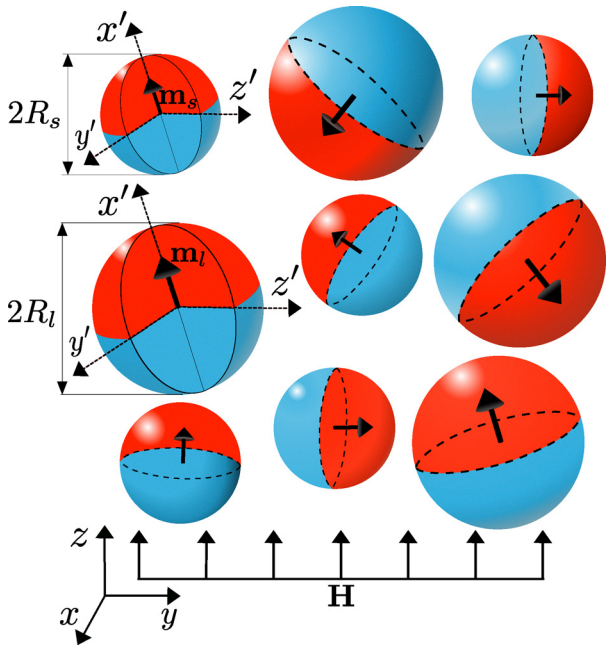

Fig. 1 A bidisperse suspension of magnetic interacting colloidal particles under an external uniform magnetic field **H**. The dark red and light blue parts of each particle represent its north and south poles, respectively.

is composed of N rigid interacting magnetic particles, divided into N_s small particles and N_l large particles, in the presence of a uniform magnetic field, the Langevin equations for translation and rotation read as follows.

$$0 = \mathbf{F}_i^{H} + \mathbf{F}_i^{M} + \sum \mathbf{F}_{ij}^{D-D} + \sum \mathbf{F}_{ij}^{R} + \mathbf{F}_i^{B}, \tag{1}$$

$$0 = \mathbf{T}_i^{H} + \mathbf{T}_i^{M} + \sum \mathbf{T}_{ij}^{D-D} + \mathbf{T}_i^{B}, \tag{2}$$

where subscripts i and j denote a generic small or large particle of the suspension. Here, $\mathbf{F}_i^{H}$ and $\mathbf{T}_i^{H}$ are the hydrodynamic drag force and torque acting on particle i, respectively; $\mathbf{F}_i^{M}$ and $\mathbf{T}_i^{M}$ are the force and torque exerted by the uniform magnetic field on particle i, respectively; $\mathbf{F}_{ij}^{D-D}$ and $\mathbf{T}_{ij}^{D-D}$ are the magnetic dipole–dipole interaction force and torque, respectively, exerted on particle i by particle j; $\mathbf{F}_{ij}^{R}$ is the repulsive force exerted by particle j on particle i to avoid particle overlapping; and $\mathbf{F}_i^{B}$ and $\mathbf{T}_i^{B}$ are the Brownian force and torque, respectively, acting on particle i.

The hydrodynamic viscous drag force, $\mathbf{F}_i^{H}$, and torque, $\mathbf{T}_i^{H}$, for a spherical particle i, with hydrodynamic radius R_i, moving with linear, $\mathbf{U}_i$, and angular, $\boldsymbol{\Omega}_i$, velocities in a Newtonian fluid are calculated as follows:[74]

$$\mathbf{F}_i^{H} = -\mathbf{R}_{\mathbf{FU}}\cdot\mathbf{U}_i, \tag{3}$$

$$\mathbf{T}_i^{H} = -\mathbf{R}_{\mathbf{T\Omega}}\cdot\boldsymbol{\Omega}_i, \tag{4}$$

where $\mathbf{R}_{\mathbf{FU}} = 6\pi\eta R_i\mathbf{I}$ and $\mathbf{R}_{\mathbf{T\Omega}} = 8\pi\eta R_i^3\mathbf{I}$ are the hydrodynamic resistance tensors, respectively, for translation and rotation, in the absence of many-body hydrodynamic interactions. Here, $\mathbf{I}$ is the unit isotropic tensor, and the i subindex adopts the notation s or l according to the type of particle (small and large, respectively). Here, many-body and lubrication hydrodynamic interactions are neglected due to the dilute regime assumed for the suspensions.

The dipole–dipole magnetic interaction force and torque exerted by the particle j on particle i, are obtained from the dipolar interaction potential[75]

$$\Phi_{ij}^{D-D}(\mathbf{r}_{ij}, \mathbf{m}_i, \mathbf{m}_j) = \frac{\mu_0}{4\pi r_{ij}^3}\left\{\mathbf{m}_i\cdot\mathbf{m}_j - \frac{3}{r_{ij}^2}(\mathbf{m}_i\cdot\mathbf{r}_{ij})(\mathbf{m}_j\cdot\mathbf{r}_{ij})\right\}, \tag{5}$$

where $\mathbf{m}_i$ and $\mathbf{m}_j$ are the dipole moments of particles i and j, respectively; $\mathbf{r}_{ij} = \mathbf{r}_i - \mathbf{r}_j$ is the separation vector between the positions of particles i and j, $r_{ij} = |\mathbf{r}_{ij}|$ is the magnitude of the vector $\mathbf{r}_{ij}$ (center distance to center distance between the particles) and μ_0 is the magnetic permeability of the free space ($\mu_0 = 4\pi \times 10^{-7}$ N A^{-2}).

The dipole–dipole magnetic interaction force and torque between the particles are then obtained by applying the translational, $\boldsymbol{\nabla} = \partial/\partial\mathbf{r}$, and rotational, $\mathcal{R} = \mathbf{u}\times\partial/\partial\mathbf{u}$ (with $\mathbf{u} = \mathbf{m}/|\mathbf{m}|$ as particle orientation), space gradient operators, respectively, to the magnetic potential as follows:

$$\mathbf{F}_{ij}^{D-D} = -\boldsymbol{\nabla}\Phi_{ij}^{D-D}, \tag{6}$$

$$\mathbf{T}_{ij}^{D-D} = -\mathcal{R}\Phi_{ij}^{D-D}. \tag{7}$$

Thus, the explicit equations for the dipole–dipole magnetic interaction force and torque, respectively, read[76,77]

$$\mathbf{F}_{ij}^{D-D} = \frac{3\mu_0}{4\pi r_{ij}^4}\{[\mathbf{m}_i\cdot\mathbf{m}_j - 5(\mathbf{m}_i\cdot\hat{\mathbf{r}}_{ij})(\mathbf{m}_j\cdot\hat{\mathbf{r}}_{ij})]\hat{\mathbf{r}}_{ij} + (\mathbf{m}_i\cdot\hat{\mathbf{r}}_{ij})\mathbf{m}_j + (\mathbf{m}_j\cdot\hat{\mathbf{r}}_{ij})\mathbf{m}_i\}, \tag{8}$$

$$\mathbf{T}_{ij}^{D-D} = -\frac{\mu_0}{4\pi r_{ij}^3}\{\mathbf{m}_i\times\mathbf{m}_j - 3(\mathbf{m}_j\cdot\hat{\mathbf{r}}_{ij})\mathbf{m}_i\times\hat{\mathbf{r}}_{ij}\}, \tag{9}$$

where $\hat{\mathbf{r}}_{ij} = \mathbf{r}_{ij}/r_{ij}$ is the unit vector of $\mathbf{r}_{ij}$.

The external magnetic field, **H**, induces a torque on the magnetic particles that reads

$$\mathbf{T}_i^{M} = -\mathcal{R}\Phi^{M}(\mathbf{m}_i, \mathbf{H}) = \mu_0(\mathbf{m}_i\times\mathbf{H}), \tag{10}$$

where $\Phi^{M}(\mathbf{m}_i, \mathbf{H}) = -\mu_0\mathbf{m}_i\cdot\mathbf{H}$ is the external magnetic potential on the i th particle. This potential also induces a magnetic force on the particles. However, in this case, it is zero, $\mathbf{F}_i^{M} = 0$, because the external magnetic field is uniform.

A repulsion potential energy is established between particles to avoid particle overlapping in the simulations. For this study, the truncated Lennard-Jones potential was chosen. This energy is expressed as follows:

$$\Phi_{ij}^{LJ}(r_{ij}) = \begin{cases} 4\epsilon\left[\left(\frac{\sigma_{ij}}{r_{ij}}\right)^{12} - \left(\frac{\sigma_{ij}}{r_{ij}}\right)^{6} + \frac{1}{4}\right], & r_{ij} < 2^{1/6}\sigma_{ij}, \\ 0, & r_{ij} \geq 2^{1/6}\sigma_{ij}, \end{cases} \tag{11}$$

where $\sigma_{ij} = R_i + R_j$, and ϵ (depth of the potential well) is assumed to be equal for any pair of suspension particles.

Then, the repulsion force to prevent particles from approaching so close is calculated by $\mathbf{F}_{ij}^{R} = -\nabla\Phi_{ij}^{LJ}(r_{ij})$, that in

turn, reads as

$$\mathbf{F}_{ij}^{\mathrm{R}}(r_{ij}) = \begin{cases} 24\epsilon\left[\dfrac{2{\sigma_{ij}}^{12}}{{r_{ij}}^{13}} - \dfrac{{\sigma_{ij}}^{6}}{{r_{ij}}^{7}}\right]\hat{\mathbf{r}}_{ij}, & r_{ij} < 2^{1/6}\sigma_{ij} \\ 0, & r_{ij} \geq 2^{1/6}\sigma_{ij}. \end{cases} \quad (12)$$

Brownian motion is due to the thermal fluctuations of the fluid molecules acting on the suspended particles *via* a stochastic force and torque called Brownian force and torque, characterized by the fluctuation–dissipation theorem[78–80]

$$\langle \mathbf{F}_i^{\mathrm{B}} \rangle = 0 \quad \text{and} \quad \langle \mathbf{F}_i^{\mathrm{B}}(0)\mathbf{F}_i^{\mathrm{B}}(t) \rangle = 2k_{\mathrm{B}}T\mathbf{R}_{\mathbf{FU}}\delta(t), \quad (13)$$

$$\langle \mathbf{T}_i^{\mathrm{B}} \rangle = 0 \quad \text{and} \quad \langle \mathbf{T}_i^{\mathrm{B}}(0)\mathbf{T}_i^{\mathrm{B}}(t) \rangle = 2k_{\mathrm{B}}T\mathbf{R}_{\mathbf{T\Omega}}\delta(t), \quad (14)$$

where $\delta(t)$ is the Dirac delta function, T is the absolute temperature of the suspension, and k_{B} is the Boltzmann constant ($k_{\mathrm{B}} = 1.380649 \times 10^{-23}$ J K^{-1}).

The translational and rotational evolution equations of the ith particle are obtained by following Ermak and McCammon's (1978)[81] approach, leading to:

$$\Delta\tilde{\mathbf{r}}_i(\tilde{t} + \Delta\tilde{t}) = \left[\sum_{j=1, j\neq i}^{N}\left(12\lambda_{ij}\tilde{\mathbf{F}}_{ij}^{\mathrm{D-D}} + \tilde{\mathbf{F}}_{ij}^{\mathrm{R}}\right)\right]\frac{\Delta\tilde{t}}{\xi_i} + \Delta\tilde{\mathbf{r}}_i^{\mathrm{B}}(\Delta\tilde{t}), \quad (15a)$$

$$\left\langle \Delta\tilde{\mathbf{r}}_i^{\mathrm{B}} \right\rangle = 0 \quad \text{and} \quad \left\langle \Delta\tilde{\mathbf{r}}_i^{\mathrm{B}}\Delta\tilde{\mathbf{r}}_i^{\mathrm{B}} \right\rangle = \frac{2}{\xi_i}\mathbf{I}\Delta\tilde{t}, \quad (15b)$$

$$\Delta\tilde{\boldsymbol{\theta}}_i(\tilde{t} + \Delta\tilde{t}) = \left[\frac{3\alpha_i}{4}\tilde{\mathbf{T}}_i^{\mathrm{M}} + \sum_{j=1, j\neq i}^{N} 9\lambda_{ij}\tilde{\mathbf{T}}_{ij}^{\mathrm{D-D}}\right]\frac{\Delta\tilde{t}}{\xi_i^3} + \Delta\tilde{\boldsymbol{\theta}}_i^{\mathrm{B}}(\Delta\tilde{t}), \quad (15c)$$

$$\left\langle \Delta\tilde{\boldsymbol{\theta}}_i^{\mathrm{B}} \right\rangle = 0 \quad \text{and} \quad \left\langle \Delta\tilde{\boldsymbol{\theta}}_i^{\mathrm{B}}\Delta\tilde{\boldsymbol{\theta}}_i^{\mathrm{B}} \right\rangle = \frac{3}{2\xi_i^3}\mathbf{I}\Delta\tilde{t}, \quad (15d)$$

where each magnitude with a tilde denotes its dimensionless form, taking the features and phenomena of the small particle as references. In this way, $\tilde{r}_i$ and $\tilde{t}$ are the dimensionless form of length r_i and time t, respectively, nondimensionalized by radius R_{s} and its corresponding translational diffusion time scale $\tau_{\mathrm{B}} = {R_{\mathrm{s}}}^2/D_{\mathrm{s}}^{\mathrm{tra}}$ ($D_{\mathrm{s}}^{\mathrm{tra}} = k_{\mathrm{B}}T/6\pi\eta R_{\mathrm{s}}$). Then, $\xi_i = R_i/R_{\mathrm{s}}$ defines the size ratio of particle $i \in \{s,l\}$; $\Delta\tilde{\mathbf{r}}_i$ and $\Delta\tilde{\boldsymbol{\theta}}_i$ are the dimensionless linear and angular displacements of the particles during the time step $\Delta\tilde{t}$; $\Delta\tilde{\mathbf{r}}_i^{\mathrm{B}}(\Delta\tilde{t})$ and $\Delta\tilde{\boldsymbol{\theta}}_i^{\mathrm{B}}(\Delta\tilde{t})$ are the random dimensionless linear and angular displacements due to Brownian motion that have zero means and covariances, $2D_i^{\mathrm{tra}}\mathbf{I}$ for translation and $2D_i^{\mathrm{rot}}\mathbf{I}$ for rotation, respectively, where $D_i^{\mathrm{tra}} = k_{\mathrm{B}}T/6\pi\eta R_i$ and $D_i^{\mathrm{rot}} = k_{\mathrm{B}}T/8\pi\eta {R_i}^3$ are the translational and rotational diffusion coefficients of a single isolated particle.

In (15a) and (15c), λ_{ij} is a dimensionless parameter that characterizes the competition between the magnetic dipole–dipole interaction of the particles i and j in contact, and the thermal energy, $k_{\mathrm{B}}T$. The dipolar coupling parameter λ_i, for a generic particle $i \in \{s,l\}$, is defined as $\lambda_i = \mu_0 {m_i}^2/16\pi {R_i}^3 k_{\mathrm{B}}T$. However, λ_{ij} is defined in terms of R_{s} according to the dimensionless process of the equations, which reads

$$\lambda_{ij} = \sqrt{(\lambda_i\xi_i^3)(\lambda_j\xi_j^3)}. \quad (16)$$

Similarly, the Langevin parameter α_i for a particle $i \in \{s,l\}$ reads

$$\alpha_i = \frac{\mu_0 m_i H}{k_{\mathrm{B}}T}, \quad (17)$$

which measures the relative interaction between the magnetic field-dipole energy of particle i and the thermal energy. The coupling parameter and Langevin parameter of large particles are related to the coupling parameter and Langevin parameter of small particles, respectively, as

$$\lambda_{\mathrm{l}} = \lambda_{\mathrm{s}}\xi^3, \quad \alpha_{\mathrm{l}} = \alpha_{\mathrm{s}}\xi^3. \quad (18)$$

The total volume fraction, $\phi = \phi_{\mathrm{s}} + \phi_{\mathrm{l}}$, is another characteristic parameter in this work. Denoting $\tilde{n}_{\mathrm{s}}$ and $\tilde{n}_{\mathrm{l}}$ as the dimensionless number densities of small and large particles, respectively, and $\phi_{\mathrm{s}} = 4\pi\tilde{n}_{\mathrm{s}}/3$, $\phi_{\mathrm{l}} = 4\pi\tilde{n}_{\mathrm{l}}\xi^3/3$ as their corresponding volume fractions, the total volume fraction of the suspension reads

$$\phi = \frac{4}{3}\pi\left(\tilde{n}_{\mathrm{s}} + \tilde{n}_{\mathrm{l}}\xi^3\right). \quad (19)$$

To establish a rigid body reference frame x'–y'–z' where the particle magnetic moments have a permanent orientation along the x'-axis as illustrated in Fig. 1, the laboratory reference frame x–y–z suffers a transformation (or three successive angular rotations) characterized by the Euler angles. These rotations are measured by a transformation matrix $\mathbf{A}$ in terms of Euler angles. Adopting a x convention (that is, second rotation about the intermediate x axis) and expressing the Euler angles in terms of the quaternions e_0, e_1, e_2, and e_3 (also known as Euler parameters) for the numerical computations free from singularities, the transformation matrix reads[82]

$$\mathbf{A} = \begin{pmatrix} {e_0}^2 + {e_1}^2 - {e_2}^2 - {e_3}^2 & 2(e_1e_2 + e_0e_3) & 2(e_1e_3 - e_0e_2) \\ 2(e_1e_2 - e_0e_3) & {e_0}^2 - {e_1}^2 + {e_2}^2 - {e_3}^2 & 2(e_2e_3 + e_0e_1) \\ 2(e_1e_3 + e_0e_2) & 2(e_2e_3 - e_0e_1) & {e_0}^2 - {e_1}^2 - {e_2}^2 + {e_3}^2 \end{pmatrix}, \quad (20)$$

where the quaternion parameters satisfy the relation ${e_0}^2 + {e_1}^2 + {e_2}^2 + {e_3}^2 = 1$.

The product of this matrix with each vector of (15c) leads to the desired transformation

$$\Delta\tilde{\theta}'_i(\tilde{t}) = \left[\frac{3\alpha_i}{4}\tilde{\mathbf{T}}_i^{\mathrm{M}'} + \sum_{j=1, j\neq i}^{N} 9\lambda_{ij}\tilde{\mathbf{T}}_{ij}^{\mathrm{D-D}'}\right]\frac{\Delta\tilde{t}}{\xi_i} + \Delta\tilde{\boldsymbol{\theta}}_i^{\mathrm{B}'}, \quad (21)$$

where the prime symbol on each vector denotes its transformation to the rigid body reference frame and $\Delta\tilde{\theta}'_i(\tilde{t}) = \tilde{\theta}'_i(\tilde{t} + \Delta\tilde{t}) - \tilde{\theta}'_i(\tilde{t})$.

Then, with $\Delta\tilde{\theta}'_i$ the quaternions of particle i can be updated to time $\tilde{t} + \Delta\tilde{t}$ as follows[83]

$$\begin{pmatrix} \Delta e_0 \\ \Delta e_1 \\ \Delta e_2 \\ \Delta e_3 \end{pmatrix} = \frac{1}{2}\begin{pmatrix} -e_1 & -e_2 & -e_3 \\ e_0 & -e_3 & e_2 \\ e_3 & e_0 & -e_1 \\ -e_2 & e_1 & e_0 \end{pmatrix} \cdot \Delta\tilde{\theta}'_i(\tilde{t}), \quad (22)$$

$$\mathbf{e}(\tilde{t}+\Delta\tilde{t}) = \frac{\mathbf{e}(\tilde{t})+\Delta\mathbf{e}}{|\mathbf{e}(\tilde{t})+\Delta\mathbf{e}|}, \tag{23}$$

where $\mathbf{e} = (e_0, e_1, e_2, e_3)$ and $\Delta\mathbf{e} = (\Delta e_0, \Delta e_1, \Delta e_2, \Delta e_3)$.

To convert any vector from the rigid body reference frame to the laboratory reference frame, it is necessary to make the product of the transposed matrix, $\mathbf{A}^{\mathrm{T}}$, by this vector. In this manner, by multiplying the matrix $\mathbf{A}^{\mathrm{T}}$ by the unit vector of $\mathbf{u}_i$, the orientation of this dipole moment is obtained in the laboratory reference frame.

4 Properties

4.1 Radial distribution function

In dimensionless terms, this property represents the ratio of the local number density at a dimensionless distance $\tilde{r}$ from a reference particle to the average number density of the suspension.

In this study, the analysis focuses on the spatial distribution of the ith-small particles surrounding each jth-large (reference) particle. This property, denoted by $g(\tilde{r})$, then reads as

$$g(\tilde{r}) = \frac{1}{4\pi\phi_{\mathrm{s}}N_{\mathrm{l}}\tilde{r}^2\Delta\tilde{r}}\left\langle \sum_{i=1}^{N_{\mathrm{l}}}\sum_{j=1}^{N_{\mathrm{s}}}\delta(\tilde{r}-\tilde{r}_{ij})\right\rangle, \tag{24}$$

where $\Delta\tilde{r}$ is the width of the dimensionless bin and $\tilde{r}_{ij}$, the dimensionless distance between particles i and j.

4.2 Magnetization

The equation to calculate the dimensionless magnetization of the suspension, $\langle\tilde{\mathbf{M}}\rangle$, as a function of time, $\tilde{t}$, of a bidisperse colloidal suspension composed of N particles reads

$$\left\langle\tilde{\mathbf{M}}(\tilde{t})\right\rangle = \frac{\sum_{i=1}^{N_{\mathrm{s}}}\tilde{\mathbf{m}}_i(\tilde{t})}{N_{\mathrm{s}}\left(1+\frac{\phi_{\mathrm{l}}}{\phi_{\mathrm{s}}}\sqrt{\frac{\lambda_{\mathrm{l}}}{\lambda_{\mathrm{s}}\xi^3}}\right)} + \frac{\sum_{j=1}^{N_{\mathrm{l}}}\tilde{\mathbf{m}}_j(\tilde{t})}{N_{\mathrm{l}}\left(1+\frac{\phi_{\mathrm{s}}}{\phi_{\mathrm{l}}}\sqrt{\frac{\lambda_{\mathrm{s}}\xi^3}{\lambda_{\mathrm{l}}}}\right)}, \tag{25}$$

where $\tilde{\mathbf{m}}_i(\tilde{t})$ and $\tilde{\mathbf{m}}_j(\tilde{t})$ are the unit vectors of the magnetic dipole moment of the small particle i and the large particle j, respectively. Here, the time-dependent magnetization has been dimensionless by the suspension saturation magnetization, M_{sat}.

5 Results

The total number of particles used in the simulations is N = 1000. The initial configuration of the system is such that the initial positions and orientations of all the particles are randomly distributed in the simulation box. The simulations are carried out in a cubic simulation box with periodic boundary conditions, where the minimum image methodology is considered.[1]

The Lennard-Jones repulsion potential is implemented in the simulations to prevent particle overlapping and agglomeration. According to test simulations and previous work,[50] the potential well $\epsilon = 100$ avoids overlapping of any pair of particles with no significant impact on the dynamics of the particles. Therefore, this value has been used in this work.

A total particle volume fraction of $\phi = 10^{-3}$ has been chosen for our simulations of dilute suspensions to ensure meaningful interparticle interactions, which would otherwise be absent in overly dilute systems. Similarly, to ensure a balanced distribution of large and small particles, the volume fraction for each has been assigned as $\phi_{\mathrm{s}} = \phi_{\mathrm{l}} = 5 \times 10^{-4}$. In addition, (18) allows one to reduce the simulation control parameters to ξ, λ_{s} and α_{s}. In view of the size range (20–100 nm) associated with single-domain ferromagnetic behavior, the size ratio ξ has been assigned values of 1, 2, and 3. The parameter λ_{s} has been selected in the range of 5 to 30, corresponding to the typical values in small particles that exhibit the aforementioned ferromagnetic behavior. Furthermore, the parameter α_{s} has been varied from 0 to 1000 to assess the influence of low and high magnetic field strengths on the clustering process and magnetization. Then, each set of values ξ–λ_{s}–α_{s} represents a bidisperse magnetic colloidal suspension (see Table 1). Five repetitions have been performed for each set to achieve good statistics in the results. The end time of the simulations is 10 000, with a time step of dimensionless units 10^{-4}.

5.1 Microstructure

Simulations of monodisperse suspensions (ξ = 1) have been carried out to depict the microstructural changes induced by the particle size difference ($\xi > 1$) in bidisperse suspensions. According to (18), the equalities $\lambda_{\mathrm{s}} = \lambda_{\mathrm{l}}$ and $\alpha_{\mathrm{s}} = \alpha_{\mathrm{l}}$ hold for $\xi = 1$.

The dipole–dipole magnetic interaction characterized by $\lambda_{\mathrm{s}} = \lambda_{\mathrm{l}} = 5$ represents a very weak interparticle interaction, which is unable to promote the clustering process.[14] This does not occur with the following values of λ_{s} used in this work.

As shown in Fig. 2, the microstructure developed for ξ = 1 and λ_{s} = 30 up to $\tilde{t}$ = 10 000 agrees with that expected.[84,85] In the absence of a magnetic field, that is, α_{s} = 0, the formation of flexible chains is initially carried out following the head-to-tail

Table 1 Set of values of size ratio (ξ), small particle dipolar coupling parameter (λ_{s}) and small particle Langevin parameter (α_{s}) used in simulations of N = 1000 particles. Each set ξ–λ_{s}–α_{s} characterizes a bidisperse magnetic colloidal suspension subject to an external uniform magnetic field

ξ	λ_{s}	α_{s}
1		0
		0.01
	5	0.03
	15	0.1
	30	0.25
		0.5
2		1
	5	1.5
	15	2.5
	30	5
		10
3		25
	5	50
	15	100
	30	300
		1000

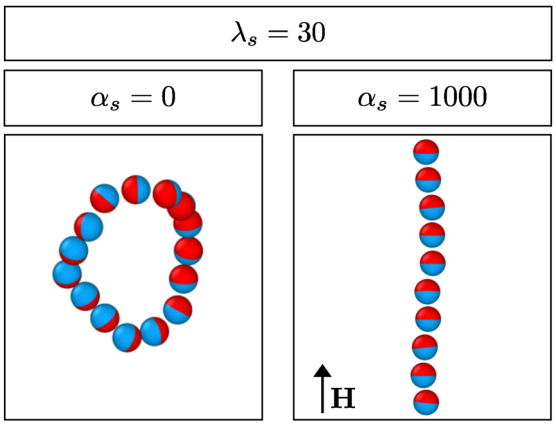

Fig. 2 Predominant microstructure in a monodisperse magnetic colloidal suspension (ξ = 1) with a magnetic dipole–dipole interaction strength characterized by λ_s = 30, in the absence of the magnetic field (α_s = 0) and exposed to a very high uniform magnetic field **H** (α_s = 1000).

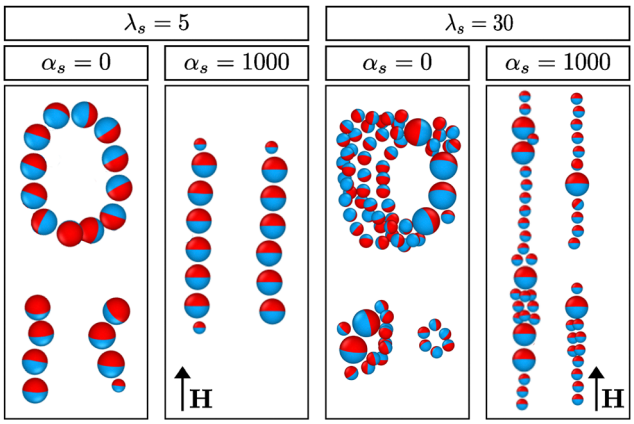

Fig. 3 Predominant microstructure in a bidisperse magnetic colloidal suspension (ξ = 2) with a magnetic dipole–dipole interaction strength characterized by λ_s = 5 and λ_s = 30, in the absence of a magnetic field (α_s = 0) and exposed to a strong uniform magnetic field **H** (α_s = 1000).

configuration. However, the thermal fluctuations over time lead them to collapse onto themselves, leading the population to consist only of rings of different sizes.[86]

In the presence of a very strong magnetic field, such as α_s = 1000 in Fig. 2, the formation of rigid chains along the magnetic field direction is carried out, which exhibit temporal growth.[14]

For bidisperse suspensions ($\xi > 1$), the difference in particle size implies different intensities of magnetic dipole moment in the particles, according to (18).

Consequently, large particles in the suspension yield strong magnetic dipole–dipole interactions with other particles and undergo a stronger interaction with the applied magnetic field. However, because of their larger sizes, thermal fluctuations diminish in large particles in comparison with small ones. Overall, this different behavior of the large particles hardly influences the interaction between them and small particles, which leads to a different microstructural behavior.

As such, in both bidisperse suspensions simulated (ξ = 2 and ξ = 3) with λ_s = 5, the dipolar interaction strength of the large particles (characterized by λ_l = 40 and λ_l = 135, respectively) induces a clustering process. The large particles interact with each other, forming rings and chains according to the applied magnetic field strength (see Fig. 3 and 4). Furthermore, their intense dipole moments also promote the adhesion of small particles to these formed chains,[87,88] as observed in Fig. 3 and 4. However, the last process occurs to a lesser extent. Hence, for dilute bidisperse suspensions with $\lambda_s < 5$, it turns out that both populations of small and large particles behave separately as if they were monodisperse suspensions.

The increase of λ_s to λ_s = 30 produces a stronger magnetic dipole–dipole interaction between particles, with λ_l = 240 for ξ = 2 and λ_l = 810 for ξ = 3. The microstructural behavior and morphology in this case are very similar to those observed for λ_s = 15. However, strengthening the interparticle interactions can promote variability with respect to the size of the cluster.

In simulations of monodisperse suspensions with λ_s = 30, each particle possesses no more than two neighboring particles due to the head-to-tail configuration. However, in simulated bidisperse suspensions, large particles can be surrounded by a larger population of small particles, as observed in Fig. 3 and 4.

This is also evidenced by Fig. 5(a), which represents the radial distribution function, $g(\tilde{r})$, for α_s = 0 of small particles around large particles at $\tilde{t}$ = 1. In this initial stage of the clustering process, the increase in the peak height of $g(\tilde{r})$ with increasing ξ for $\tilde{r}$ close to 1 implies a larger number of small particles attached to the large ones. This is consistent with the stronger magnetic interaction displayed by the latter as well as their larger surface.

Then, as occurs in monodisperse suspensions, the cluster population in the bidisperse suspensions for α_s = 0 comprises only closed structures, involving small and large particles. However, these clusters begin to emerge from open structures consisting of large particles linked to short chains of small ones. This corresponds to the peaks observed in Fig. 5(b) for $\tilde{t}$ = 100 at $\tilde{r}$ close to 1 and 3.

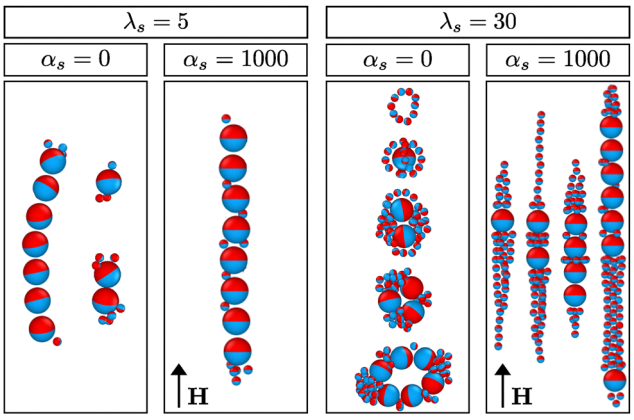

Fig. 4 Predominant microstructure in a bidisperse magnetic colloidal suspension (ξ = 3) with a magnetic dipole–dipole interaction strength characterized by λ_s = 5 and λ_s = 30, in the absence of a magnetic field (α_s = 0) and exposed to a uniform magnetic field **H** (α_s = 1000).

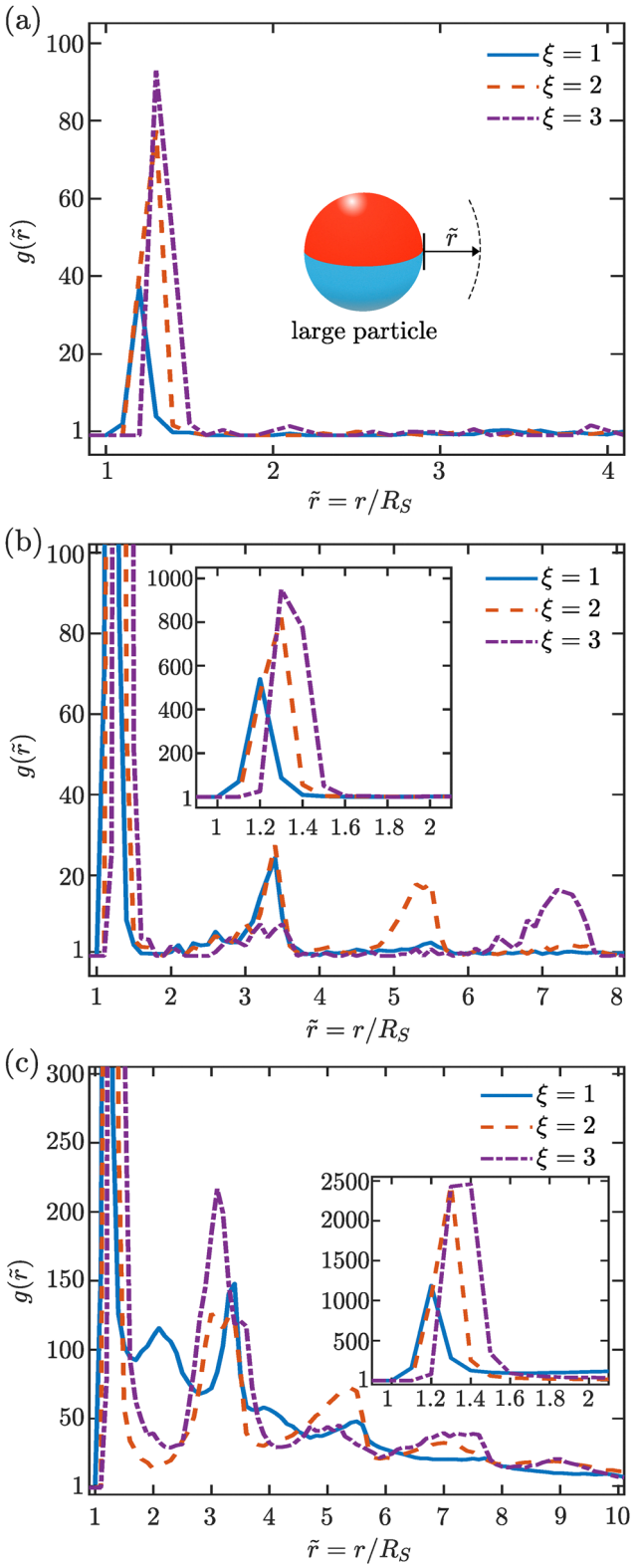

Fig. 5 Radial distribution function, $g(\tilde{r})$, of small particles around large ones in monodisperse (ξ = 1) and bidisperse (ξ = 2; ξ = 3) magnetic colloidal suspensions (λ_s = 30; α_s = 0). The dimensionless distance $\tilde{r} = r/R_s$ is measured from the surface of the large particles. The radial distribution function is plotted at (a) $\tilde{t}$ = 1, (b) $\tilde{t}$ = 100 and (c) $\tilde{t}$ = 10 000.

The absence of a peak at this final value of $\tilde{r}$ for ξ = 3 is due to the stronger magnetic force and the larger surface area of the large particles. These factors allow the small ones to come even closer, breaking their chain formation. In contrast, the presence of peaks at $\tilde{r} \approx 5$ for ξ = 2 and at $\tilde{r} \approx 7$ for ξ = 3 arises from the clustering process of large particles. Therefore, these peaks correspond to the most distant small particles that are aggregated to large particles that neighbor the large reference particles.

Afterward, the strong magnetic interaction between particles in the same cluster triggers its collapse observed in Fig. 3 and 4. However, despite the strong attraction offered by the large particles on the small ones, this does not prevent the formation of clusters composed of only small particles, which consists of small rings and chains. However, in the course of time, most of them have incorporated into structures containing large particles as a result of the strong local attraction induced by the latter.

The thriving formation of closed structures leads to the agglomeration of more small particles around the large ones, as shown by the higher values of $g(\tilde{r})$ in Fig. 5(c), which corresponds to $\tilde{t}$ = 10 000.

The presence of significant peaks in $\tilde{r} \approx 2$ and $\tilde{r} \approx 3$ for ξ = 1 is correlated with the formation of small rings and the prevalence of the head-to-tail configuration, respectively. However, the prominent peaks observed at $\tilde{r} \approx 3$ for ξ = 2 and ξ = 3 imply the assembly of at least two layers of small particles on the magnetic poles of the large particles (see Fig. 3 and 4 for α_s = 0). The appearance of additional peaks at higher values of $\tilde{r}$ corresponds to the population of small particles surrounding the large particles that are neighbors of the reference large particles, as previously explained.

A very interesting cluster obtained in the simulations for ξ = 3 is the structure composed of one large particle and several small particles, as observed in Fig. 4. This is a shell-like structure and clearly shows the impact of the particle size difference in a bidisperse magnetic suspension. The small particles tend to align in the opposite direction of the magnetic dipole moment of the large particle due to the non-uniform local magnetic field produced by the latter. Then, the small particles are arranged according to the corresponding local magnetic field lines. The importance of this aggregation mechanism, which is observed even for moderate magnetic field strengths, that is, $0 < \alpha_s < 1$, will be discussed in the next section.

Finally, the increase of α_s to 1000 leads all the magnetic dipole moments of the particles to align with the direction of the applied magnetic field. This implies that all the dipole moments adopt a parallel configuration, which favors magnetic dipole–dipole interactions. In addition, the high values of α_s imply that the stronger uniform magnetic field screens the local field, avoiding the formation of shell-like structures. However, the presence of intense local magnetic fields is still evidenced due to the formation of bulk chains between large particles as observed for α_s = 1000 and both values of ξ.

5.2 Magnetization

A general analysis of the magnetization $\langle \tilde{\mathbf{M}}(\tilde{t}) \rangle$ (25) of the simulated suspensions reveals that the x- and y-components

of $\langle \tilde{\mathbf{M}}(\tilde{t}) \rangle$ are constantly zero over time. Therefore, $\langle \tilde{\mathbf{M}}(\tilde{t}) \rangle$ relies solely on its z component, $\langle \tilde{\mathbf{M}}(\tilde{t}) \rangle_z$, which is now denoted as $\langle \tilde{M}(\tilde{t}) \rangle$.

The temporal behavior of $\langle \tilde{M}(\tilde{t}) \rangle$ in monodisperse suspensions ($\xi = 1$) is depicted in Fig. 6(a)–(c). The saturation behavior of $\langle \tilde{M}(\tilde{t}) \rangle$ quickly achieved for $\lambda_s = 5$ (see Fig. 6(a)) is related to the absence of the clustering process. The isolated behavior of the particles allows, on average, rapid balance of the effect of the uniform magnetic field $\mathbf{H}$ and thermal fluctuations on the orientations of their magnetic dipole moments. Then, the resulting equilibrium values of $\langle \tilde{M}(\tilde{t}) \rangle$ coincide with Langevin magnetization.[89]

In contrast, the development of the clustering process for $\lambda_s = 15$ and $\lambda_s = 30$ leads to pronounced transient behavior of $\langle \tilde{M}(\tilde{t}) \rangle$ in moderate magnetic fields ($0 \leq \alpha_s \leq 5$). The bond between particles induces their magnetic dipole moments to

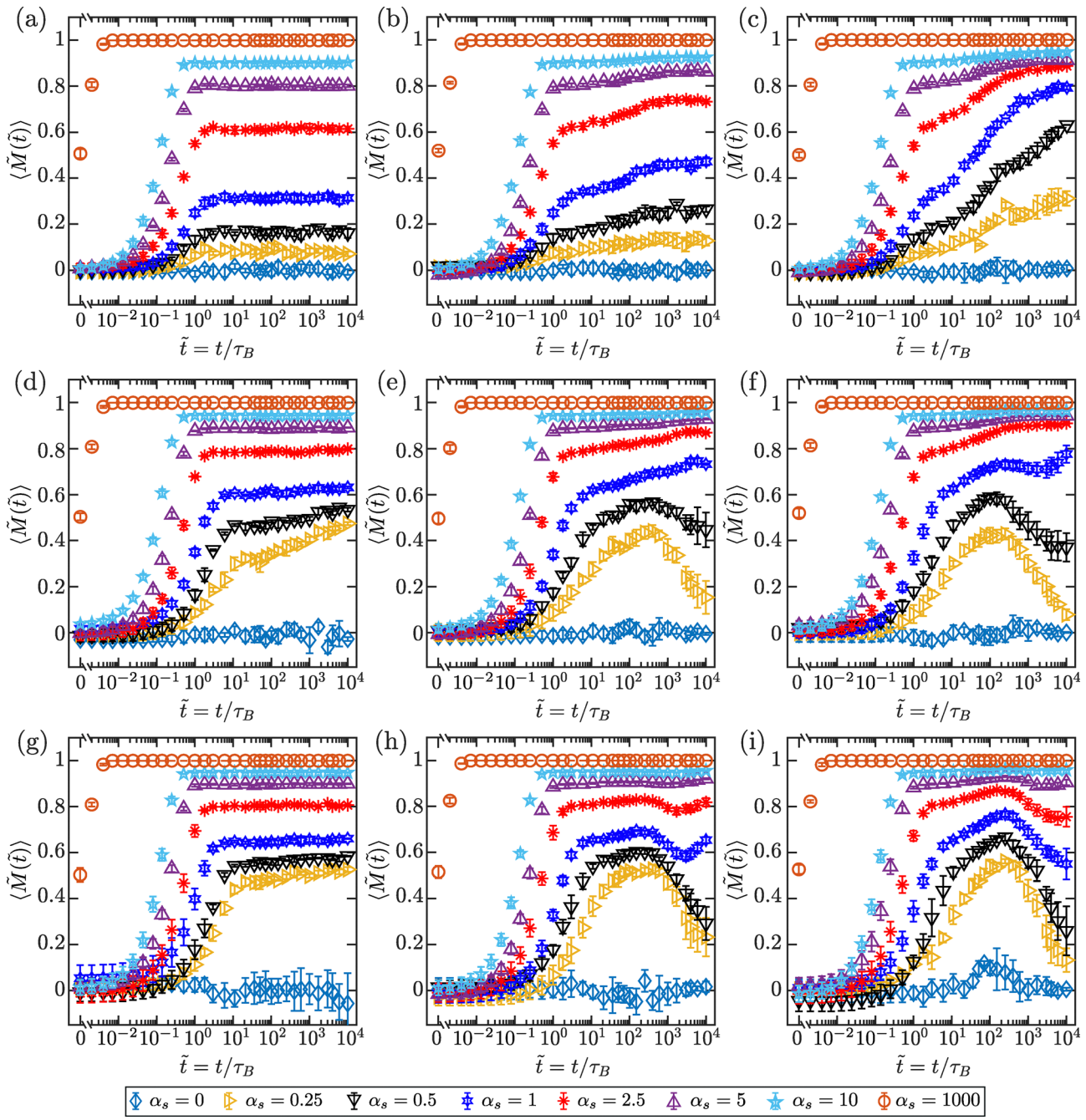

Fig. 6 Temporal evolution of magnetization, $\langle \tilde{M}(\tilde{t}) \rangle$, of a magnetic colloidal suspension along the applied magnetic field direction. The curves in the figures corresponds to monodisperse, $\xi = 1$ (a)–(c), and bidisperse suspensions with $\xi = 2$ (d)–(f) and $\xi = 3$ (g)–(i) for $\lambda_s = 5$ (a), (d) and (g), $\lambda_s = 15$ (b), (e) and (h) and $\lambda_s = 30$ (c), (f) and (i). The uniform magnetic fields applied on the suspensions are characterized by α_s, whose values are given at the bottom of the plots.

adopt similar orientations. In the absence of a magnetic field ($\alpha_s = 0$), thermal fluctuations lead particles and clusters to exhibit continuous random rotation until they collapse into rings, which, on average, produces $\langle \tilde{M}(\tilde{t}) \rangle = 0$ throughout the entire clustering process.[90]

However, as the strength of the applied magnetic field increases, their orientations approach that of the magnetic field. This involves the formation of flexible chains along the magnetic field direction, which, in turn, implies the enhancement of $\langle \tilde{M}(\tilde{t}) \rangle$ over time. Moreover, the increase of λ_s from 15 to 30 implies a strengthening of the particle bond that leads to the increase of $\langle \tilde{M}(\tilde{t}) \rangle$ as observed in Fig. 6(b) and (c).

Furthermore, in the case of a very strong magnetic field such as $\alpha_s = 1000$, the alignment between all the magnetic dipole moments and the magnetic field is nearly perfect at the onset of the clustering process. Therefore, the latter do not have a significant influence of $\langle \tilde{M}(\tilde{t}) \rangle$ over time. These results are used as a reference frame for the analysis of the temporal behavior of $\langle \tilde{M}(\tilde{t}) \rangle$ in bidisperse suspensions ($\xi > 1$).

The analysis of bidisperse suspensions begins with the case of $\lambda_s = 5$. Regardless of the ξ value, the clustering process of large particles rapidly progresses due to their strong magnetic dipole–dipole interaction. Then, regarding the poor aggregation of small particles with large ones, $\langle \tilde{M}(\tilde{t}) \rangle$ approaches saturation behavior quickly. However, due to the development of the clustering process with large particles, the observed saturation values of $\langle \tilde{M}(\tilde{t}) \rangle$ do not coincide with their corresponding Langevin magnetization values.

However, because of the higher α_l values and weak random rotation of the large particles, their intense magnetic dipole moments tend to exhibit a better alignment with the magnetic field direction even at low α_s values. This gives rise to a substantial enhancement of $\langle \tilde{M}(\tilde{t}) \rangle$ for $\xi = 2$ and $\xi = 3$ compared to the monodisperse case for moderate α_s, shown in Fig. 6(a), (d) and (g).

In case of high α_s values, such as $\alpha_s = 1000$, the near-perfect alignment of particle dipole moments with the magnetic field causes a similar temporal behavior of $\langle \tilde{M}(\tilde{t}) \rangle$ for bidisperse and monodisperse suspensions.

As occurs in the monodisperse case, the clustering process developed with $\lambda_s = 15$ and $\lambda_s = 30$ in bidisperse suspensions gives rise to long transient behavior of $\langle \tilde{M}(\tilde{t}) \rangle$, as shown in Fig. 6(e), (f), (h) and (i). However, as happens with $\lambda_s = 5$ at moderate values of α_s, the stronger sensitivity of the large particles to the applied magnetic field causes an improvement of $\langle \tilde{M}(\tilde{t}) \rangle$ over the corresponding monodisperse case at the initial stage of the clustering process. This is evidenced in Fig. 7, where the very high initial contribution of the large particles to magnetization is shown, Fig. 7(b), compared to that of the small particles, Fig. 7(a).

However, around $\tilde{t} = 100$, the growth over time of $\langle \tilde{M}(\tilde{t}) \rangle$ ceases and begins to decline. In general, because both small and large particles contribute to the reduction of $\langle \tilde{M}(\tilde{t}) \rangle$ as observed in Fig. 7(a) and (b), this decay can be attributed to the formation of the closed structures mentioned above. This is because such a structure involves the reduction of the magnetic dipole moments along the magnetic field direction.

For $\xi = 2$, all closed structures comprise more than one large particle, which is able to close itself by acquiring small particles. The net contribution of their magnetic dipole moments to $\langle \tilde{M}(\tilde{t}) \rangle$ becomes negligible. Therefore, with the progress of closed structure formation, the intense magnetic dipole moments of the large particles no longer impact $\langle \tilde{M}(\tilde{t}) \rangle$, and this begins to wane.

For $\xi = 3$, the decay of $\langle \tilde{M}(\tilde{t}) \rangle$ corresponds to the formation of shell-like structures. The most basic formation process is depicted in Fig. 8 and shown in the Videos V1 and V2 of the ESI.† Although the figure shows this formation for $\alpha_s = 0$, this is also observed for $0 < \alpha_s \leq 1$. According to the figure, up to

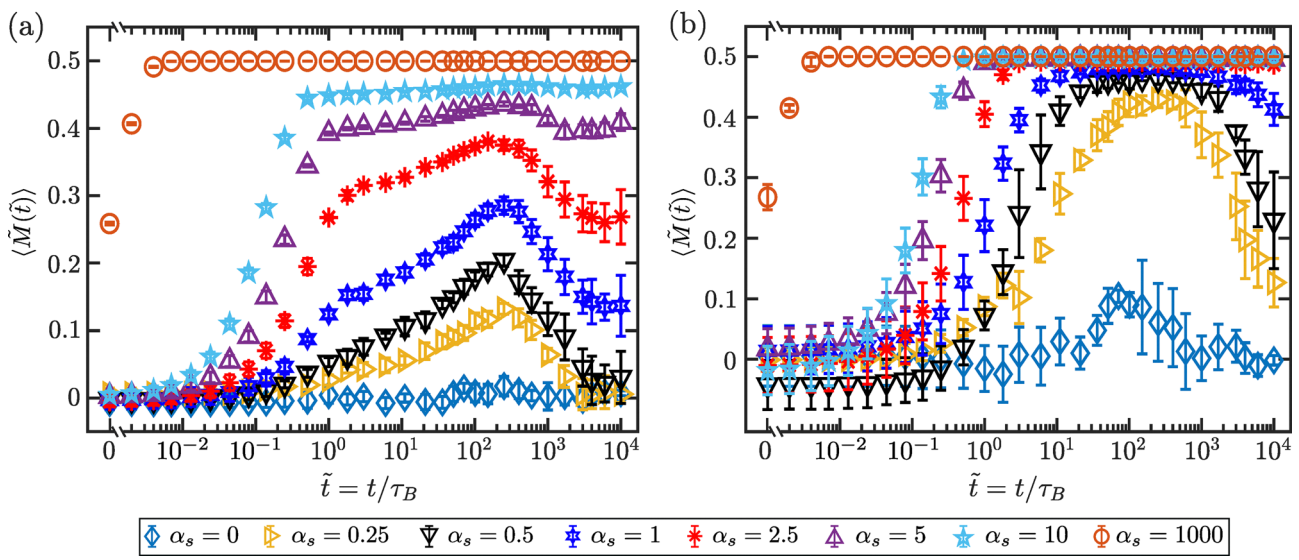

Fig. 7 Contribution to the temporal evolution of magnetization, $\langle \tilde{M}(\tilde{t}) \rangle$, derived from (a) small particles and (b) large particles along the applied magnetic field direction. The curves in both figures correspond to a bidisperse suspension with $\xi = 3$ and $\lambda_s = 30$. The magnetic fields applied on the suspensions are characterized by α_s, whose values are given at the bottom of the plots.

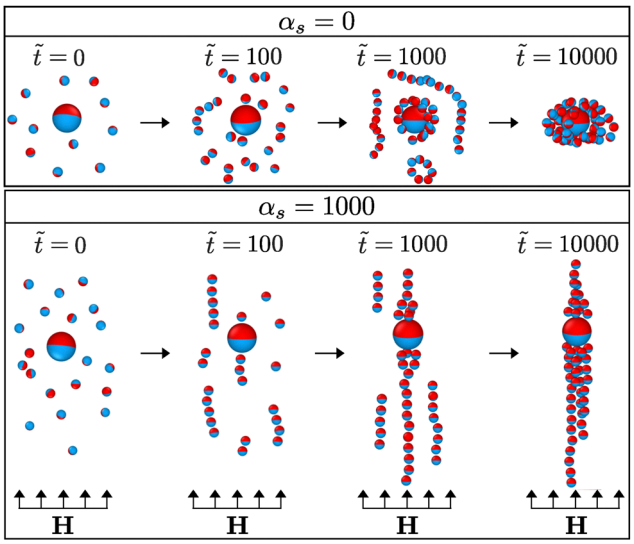

Fig. 8 Aggregation process of small particles around a large particle in a bidisperse magnetic colloidal suspension with size ratio ξ = 3 and a high interparticle dipolar interaction (λ_s = 30 and λ_l = 810). The upper panel shows the formation of a shell-like structure in the absence of a magnetic field (α_s = 0) and the lower panel shows the basic structure formed under a very high magnetic field (α_s = 1000). Videos of the formation of these clusters are shown in the ESI.†

$\tilde{t}$ = 100 a large particle has captured a few small particles. Due to its high sensitivity, large particles tend to easily align with the applied magnetic field ($\alpha_s > 0$), which also induces this alignment on small particles. This explains the very high increase in $\langle \tilde{M}(\tilde{t}) \rangle$ compared to the monodisperse suspension. However, for $100 < \tilde{t} < 10\,000$, more small particles surround the large one and form a shell-like structure. The aforementioned relative orientation of the small particles in relation to the large particle leads to the decay of $\langle \tilde{M}(\tilde{t}) \rangle$ observed during this time period.

Finally, for a strong magnetic field strength, *i.e.* $\alpha_s > 1$, the large particles achieve a perfect alignment with the magnetic field direction since, according to Fig. 7(b), they exhibit the maximum possible contribution to $\langle \tilde{M}(\tilde{t}) \rangle$. However, depending on the intensity of their magnetic dipole moments, their local field can still compete against the applied external field. This can affect the orientation of small particles and provoke a slight decay of $\langle \tilde{M}(\tilde{t}) \rangle$, as observed for ξ = 3 with α_s = 2.5 in Fig. 6(h) and (i). In the case of very strong magnetic fields, such as α_s = 1000, the clustering process does not influence the growth of $\langle \tilde{M}(\tilde{t}) \rangle$ because, as observed in Fig. 8, the clusters change over time, but all the particles are perfectly aligned with the magnetic field direction.

6 Conclusions

Using BD simulations, the influence of particle size differences, ξ, in bidisperse magnetic colloidal suspensions on their microstructure and magnetization over time has been investigated. Regarding the dilute regime, the total particle volume fraction of suspensions ($\phi = 10^{-3}$) is fairly distributed between small and large particles ($\phi_s = \phi_l = 5 \times 10^{-4}$). In addition, assuming proportionality between the magnetic dipole moment of the particle and its volume, the parameters related to small particles are used as simulation parameters.

The high magnetic dipole moment intensities of large particles in bidisperse suspensions cause variability in the microstructure compared to monodisperse suspensions, which show rings and chains, depending on the value of α_s. Also, depending on the magnetic dipole–dipole interaction strength (λ_s), the clustering process in bidisperse suspensions develops primarily with large particles (λ_s = 5) or with large and small particles (λ_s = 15, λ_s = 30). In the latter case, the significant magnetic dipole moment of a large particle is capable of attracting numerous small particles, evidenced by a temporal increase of the radial distribution function of small particles around the large ones. This improves as λ_s increases. In general, large particles in a bidisperse suspension function as junction points of small particles. As a particular case, for ξ = 3, the magnetic dipole moment of large particles strengthens, causing small particles to form shells around large ones following the local magnetic field lines generated by the latter.

The uniform magnetic field applied, characterized by α_s, affects the orientation of the structures. Low values of α_s allow the formation of flux-closure structures such as rings and shells. In contrast, high α_s leads to linear clusters along the magnetic field direction, such as bulk chains comprising small particles on the magnetic poles of the large ones.

Variability in microstructure affects the temporal behavior of magnetization, $\langle \tilde{M}(\tilde{t}) \rangle$, in bidisperse suspensions irrespective of the value ξ. As a result of the higher magnetic dipole moment intensity of the large particles, despite α_s taking low values, the assumption initially mentioned leads to a high α_s, which means a strong interaction between the large particles and the applied uniform magnetic field. Then, the magnetic dipole moments of these particles adopt a near-magnetic field alignment with the magnetic field direction at the first stages of the clustering process ($\tilde{t}$ = 100). Additionally, because of their larger sizes, thermal fluctuations weakly disturb the orientation of large particles. Both facts improve substantially $\langle \tilde{M}(\tilde{t}) \rangle$ compared to monodisperse suspensions. Afterward, the large particles continue to aggregate and with the small particles. For low values of α_s, such as $\alpha_s < 1$, the very strong interaction between particles in the same cluster leads to the collapse of this into a closed structure, which occurs mainly at $\tilde{t} > 100$. Then, the progressive formation of these structures, including rings and shell-like structures, decreases $\langle \tilde{M}(\tilde{t}) \rangle$ over time in a bidisperse suspension. For cases with $\alpha_s > 1$, large particles can preserve their perfect alignment with the magnetic field, and the remnant decay still observed in the temporal evolution of $\langle \tilde{M}(\tilde{t}) \rangle$ is entirely caused by small particles, which remain strongly affected by the local magnetic field of large particles. For very high values of α_s, such as α_s = 1000, the clustering process does not affect the behavior of $\langle \tilde{M}(\tilde{t}) \rangle$ due to the perfect alignment of all magnetic dipole moments of the particles along the field direction.

Author contributions

Luis R. Pérez-Marcos: conceptualization, formal analysis, methodology, writing – original draft, and writing – review & editing. Ronal A. DeLaCruz-Araujo: funding acquisition, conceptualization, and supervision. Heberth A. Diestra-Cruz: funding acquisition, conceptualization, and supervision. Obidio Rubio: funding acquisition, resources, and supervision. Ubaldo M. Córdova-Figueroa: resources and supervision. Glenn C. Vidal-Urquiza: funding acquisition, conceptualization, supervision, and writing – review & editing.

Conflicts of interest

There is no conflicts of interest.

Data availability

The data for this article, specifically used for each figure, are available in Zenodo at **https://doi.org/10.5281/zenodo.15627512**.

Acknowledgements

This work was subsidized by CONCYTEC through the PROCIENCIA program within the framework of the contest ''Basic Research Projects 2021-01'', according to contract no. 041-2021-FONDECYT. In addition, the authors acknowledge Boqueron HPCf from the University of Puerto Rico for the computational support provided for some simulations performed in this research work. Finally, Luis R. Pérez-Marcos thanks the Center for the Advancement of Wearable Technologies (CAWT) for the partial financial support through the NSF Grant No. OIA-1849243.

References

1 A. Satoh, *Introduction to molecular-microsimulation for colloidal dispersions*, Elsevier, 2003.
2 M. Waarden, *J. Colloid Sci.*, 1950, **5**, 317–325.
3 E. Mackor, *J. Colloid Sci.*, 1951, **6**, 492–495.
4 R. Rosensweig, J. Nestor and R. Timmins, *Materials associated with direct energy conversion*, 1965.
5 T. McIntosh, A. Magid and S. Simon, *Biochemistry*, 1987, **26**, 7325–7332.
6 R. Brown, London (not published), 1827.
7 A. Einstein, *Investigations on the Theory of the Brownian Movement*, Courier Corporation, 1956.
8 W. Russel, *Annu. Rev. Fluid Mech.*, 1981, **13**, 425–455.
9 S. Odenbach, *Colloidal magnetic fluids: basics, development and application of ferrofluids*, Springer Science & Business Media, 2009, vol. 763.
10 R. E. Rosensweig, *Ferrohydrodynamics*, Courier Corporation, 2013.
11 L. N. Donselaar, P. M. Frederik, P. Bomans, P. A. Buining, B. M. Humbel and A. P. Philipse, *J. Magn. Magn. Mater.*, 1999, **201**, 58–61.
12 N. Kovalchuk and V. Starov, *Adv. Colloid Interface Sci.*, 2012, **179**, 99–106.
13 A. Tomilov, A. Videcoq, M. Cerbelaud, M. A. Piechowiak, T. Chartier, T. Ala-Nissila, D. Bochicchio and R. Ferrando, *J. Phys. Chem. B*, 2013, **117**, 14509–14517.
14 J. Faraudo, J. S. Andreu, C. Calero and J. Camacho, *Adv. Funct. Mater.*, 2016, **26**, 3837–3858.
15 J. Thomas, *J. Appl. Phys.*, 1966, **37**, 2914–2915.
16 R. Chantrell, A. Bradbury, J. Popplewell and S. Charles, *J. Phys. D: Appl. Phys.*, 1980, **13**, L119.
17 V. S. Mendelev and A. O. Ivanov, *Phys. Rev. E: Stat., Nonlinear, Soft Matter Phys.*, 2004, **70**, 051502.
18 M. Matsuzaki, H. Kikura, J. Matsushita, M. Aritomi and H. Akatsuka, *Sci. Technol. Adv. Mater.*, 2004, **5**, 667–671.
19 M. Klokkenburg, C. Vonk, E. M. Claesson, J. D. Meeldijk, B. H. Erné and A. P. Philipse, *J. Am. Chem. Soc.*, 2004, **126**, 16706–16707.
20 N. Mousavi, S. D. Khapli and S. Kumar, *J. Appl. Phys.*, 2015, **117**, 103907.
21 A. Y. Zubarev and L. Y. Iskakova, *J. Exp. Theor. Phys.*, 1995, **80**, 857–866.
22 A. Darras, E. Opsomer, N. Vandewalle and G. Lumay, *Eur. Phys. J. E: Soft Matter Biol. Phys.*, 2019, **42**, 1–9.
23 C. F. Hayes, *J. Colloid Interface Sci.*, 1975, **52**, 239–243.
24 B. Jeyadevan and I. Nakatani, *J. Magn. Magn. Mater.*, 1999, **201**, 62–65.
25 M. Barrett, A. Deschner, J. P. Embs and M. C. Rheinstädter, *Soft Matter*, 2011, **7**, 6678–6683.
26 J. Zhang, M. R. Hassan, B. Rallabandi and C. Wang, *Soft Matter*, 2019, **15**, 2439–2446.
27 C. Lang and M. P. Lettinga, *Macromolecules*, 2020, **53**, 2662–2668.
28 Y. Kawabata, S. Ishida and Y. Imai, *Phys. Fluids*, 2024, **36**, 033353.
29 E. Hasmonay, E. Dubois, S. Neveu, J.-C. Bacri and R. Perzynski, *Eur. Phys. J. B*, 2001, **21**, 19–29.
30 A. O. Ivanov and S. S. Kantorovich, *Phys. Rev. E: Stat., Nonlinear, Soft Matter Phys.*, 2004, **70**, 021401.
31 G. Mériguet, M. Jardat and P. Turq, *J. Chem. Phys.*, 2005, **123**, 144915.
32 M. Shliomis, *et al.*, *Zh. Eksp. Teor. Fiz.*, 1972, **61**, 2411–2418.
33 B. Felderhof, *Phys. Rev. E: Stat. Phys., Plasmas, Fluids, Relat. Interdiscip. Top.*, 2000, **62**, 3848.
34 P. Ilg, M. Kröger and S. Hess, *Phys. Rev. E: Stat., Nonlinear, Soft Matter Phys.*, 2005, **71**, 051201.
35 M. Gerth-Noritzsch, D. Y. Borin and S. Odenbach, *J. Phys.: Condens. Matter*, 2011, **23**, 346002.
36 K. Shahrivar, J. R. Morillas, Y. Luengo, H. Gavilan, P. Morales, C. Bierwisch and J. de Vicente, *J. Rheol.*, 2019, **63**, 547–558.
37 J. R. Morillas and J. de Vicente, *Soft Matter*, 2020, **16**, 9614–9642.
38 J. Li, Y. Huang, X. Liu, Y. Lin, L. Bai and Q. Li, *Sci. Technol. Adv. Mater.*, 2007, **8**, 448–454.
39 M. Klokkenburg, B. H. Erné, V. Mendelev and A. Ivanov, *J. Phys.: Condens. Matter*, 2008, **20**, 204113.

40 G. A. Roure and F. R. Cunha, *J. Magn. Magn. Mater.*, 2020, **513**, 167082.
41 N. Wereley, *Magnetorheology: advances and applications*, Royal Society of Chemistry, 2014.
42 P. Zhang, M. Kamezaki, K. Otsuki, Z. He, H. Sakamoto and S. Sugano, 2019 IEEE/ASME International Conference on Advanced Intelligent Mechatronics (AIM), 2019, pp. 400–405.
43 D. N. Rao Miriyala and P. Goyal, *arXiv*, 2022, preprint, arXiv:2201.09027, DOI: **10.48550/arXiv.2201.09027**.
44 B. F. Spencer Jr, G. Yang, J. D. Carlson and M. K. Sain, Proceedings of the second world conference on structural control, 1998, pp. 417–426.
45 N. K. Rai, G. Reddy, S. Ramanujam, V. Venkatraj and P. Agrawal, *Def. Sci. J.*, 2009, **59**, 239–251.
46 T. Sakurai and S. Morishita, *Front. Mech. Eng.*, 2017, **12**, 224–233.
47 F. Xiong, S. Huang and N. Gu, *Drug Dev. Ind. Pharm.*, 2018, **44**, 697–706.
48 E. E. Etli and A. Akar, *Medicine*, 2022, **11**, 934–941.
49 P. Tierno, *Phys. Chem. Chem. Phys.*, 2014, **16**, 23515–23528.
50 G. I. Vega-Bellido, R. A. DeLaCruz-Araujo, I. Kretzschmar and U. M. Córdova-Figueroa, *Soft Matter*, 2019, **15**, 4078–4086.
51 J. A. Victoria-Camacho, R. A. DeLaCruz-Araujo, I. Kretzschmar and U. M. Córdova-Figueroa, *Soft Matter*, 2020, **16**, 2460–2472.
52 J. J. Bradley, V. A. Martinez, J. Arlt, J. R. Royer and W. C. Poon, *Soft Matter*, 2023, **19**, 8179–8192.
53 R. Rosensweig, *J. Magn. Magn. Mater.*, 2019, **479**, 301–306.
54 D. K. Mohapatra, P. J. Camp and J. Philip, *Nanoscale Adv.*, 2021, **3**, 3573–3592.
55 D. I. Radushnov, A. Y. Solovyova and E. A. Elfimova, *Polymers*, 2023, **15**, 2678.
56 J. Huang, Z. Wang and C. Holm, *J. Magn. Magn. Mater.*, 2005, **289**, 234–237.
57 P. Camp, E. Elfimova and A. Ivanov, *J. Phys.: Condens. Matter*, 2014, **26**, 456002.
58 G. Bossis, A. Ciffreo, Y. Grasselli and O. Volkova, *Rheol. Acta*, 2023, **62**, 205–223.
59 J. G. de Falco Manuel, A. J. F. Bombard and E. R. Weeks, *Smart Mater. Struct.*, 2023, **32**, 045014.
60 Y. Rabbani, N. Hajinajaf and M. Shariaty-Niassar, *J. Intell. Mater. Syst. Struct.*, 2023, **34**, 1715–1738.
61 A. O. Ivanov and P. J. Camp, *Phys. Rev. E*, 2023, **107**, 034604.
62 V. Ogarko and S. Luding, *J. Chem. Phys.*, 2012, **136**, 124508.
63 V. Ogarko and S. Luding, *Soft Matter*, 2013, **9**, 9530–9534.
64 Y. Fu, J. Yao, H. Zhao, G. Zhao and Y. Qiu, *Soft Matter*, 2019, **15**, 6867–6877.
65 M. Kostoglou and T. D. Karapantsios, *Colloids Interfaces*, 2024, **8**, 7.
66 A. Zubarev and L. Iskakova, *Colloid J.*, 2003, **65**, 711–719.
67 Z. Wang and C. Holm, *Phys. Rev. E: Stat., Nonlinear, Soft Matter Phys.*, 2003, **68**, 041401.
68 J. Huang and C. Holm, *Phys. Rev. E: Stat., Nonlinear, Soft Matter Phys.*, 2004, **70**, 061404.
69 D. Irfachsyad and H. Meidia, *Mater. Sci. Forum*, 2020, 283–289.
70 D. Susan-Resiga, V.-M. Socoliuc, I. Borbáth, T. Borbáth, S. C. Tripon, F. Balanean and L. Vékás, *Soft Matter*, 2024, **20**, 6176–6192.
71 E. Sheldeshova, A. Churaev and P. Ryapolov, *Fluids*, 2023, **8**, 47.
72 M. Jadav and S. Bhatnagar, *J. Magn. Magn. Mater.*, 2024, **590**, 171614.
73 W. Coffey and Y. P. Kalmykov, *The Langevin equation: with applications to stochastic problems in physics, chemistry and electrical engineering*, World Scientific, 2012, vol. 27.
74 G. G. Stokes, *et al.*, *Mathematical and Physical Papers*, 1851, pp. 1880–1905.
75 S. Chikazumi and C. D. Graham, *Physics of ferromagnetism*, Oxford University Press, 1997.
76 P. B. Landecker, D. D. Villani and K. W. Yung, *Magn. Electr. Sep.*, 1970, **10**, 29–33.
77 A. Satoh, *Modeling of magnetic particle suspensions for simulations*, CRC Press, 2017.
78 H. Nyquist, *Phys. Rev.*, 1928, **32**, 110.
79 R. Kubo, *Rep. Prog. Phys.*, 1966, **29**, 255.
80 R. Kubo, *Science*, 1986, **233**, 330–334.
81 D. L. Ermak and J. A. McCammon, *J. Chem. Phys.*, 1978, **69**, 1352–1360.
82 H. Goldstein, C. Poole and J. Safko, *Classical mechanics*, 2002.
83 D. J. Evans and S. Murad, *Mol. Phys.*, 1977, **34**, 327–331.
84 P. De Gennes and P. Pincus, *Phys. Kondens. Mater.*, 1970, **11**, 189–198.
85 A. Pshenichnikov and V. Mekhonoshin, *J. Magn. Magn. Mater.*, 2000, **213**, 357–369.
86 S. L. Tripp, S. V. Pusztay, A. E. Ribbe and A. Wei, *J. Am. Chem. Soc.*, 2002, **124**, 7914–7915.
87 A. Ivanov and S. Kantorovich, *Colloid J.*, 2003, **65**, 166–176.
88 E. Siebert, V. Dupuis, S. Neveu and S. Odenbach, *J. Magn. Magn. Mater.*, 2015, **374**, 44–49.
89 P. Langevin, *J. Phys. Theor. Appl.*, 1905, **4**, 678–693.
90 L. Gutiérrez, L. De la Cueva, M. Moros, E. Mazaro, S. De Bernardo, J. M. De la Fuente, M. P. Morales and G. Salas, *Nanotechnology*, 2019, **30**, 112001.

